A Density Functional Theory Study of the Topology of the Charge Density of Complexes of 8-Hydroxyquinoline with Mn(III), Fe(III), and Co(III)

Juan Murgich* and Héctor J. Franco†

Centro de Química, Instituto Venezolano de Investigaciones Científicas (IVIC), Apartado 21827, Caracas 1020A, Venezuela, and Escuela de Química, Universidad Central de Venezuela, Apartado 47102, Caracas 1041, Venezuela

Received: January 12, 2009; Revised Manuscript Received: February 26, 2009

By use of the quantum theory of atoms in molecules, it was found that the electronic charge distribution $\rho(\mathbf{r})$ of the metal atoms in Mn(III), Fe(III), and Co(III) complexes of 8-hydroxyquinoline (8HQ) showed eight nonbonded concentrations in their valence shell that were located at the corners of a cube and a depletion region was located in each of its six faces. Coordination was such that regions of charge concentration of the ligands matched the depletion ones of the metal. The O− and N−metal bonds showed low $\rho(\mathbf{r}_c)$ values at the bond critical point $\mathbf{r}_c$ and low and positive ones for its Laplacian indicating that they were dative bonds of close shell type with a degree of covalency. Most changes in ρ(r) were located around the N and O atoms of 8HQ directly involved in dative bonds. By use of the delocalization index $\delta(C_A,C_B)$ only for C−C bonds, it was found that coordination increased the aromaticity of most of them. The most important changes in $\rho(\mathbf{r})$ were found in the C−H bonds were a noticeable increase in bond strength was obtained upon coordination.

Introduction

8-Hydroxyquinoline (8HQ) is a well-known chelating agent, extensively used in analytical chemistry[1−4] (see Figure 1). When its OH group is deprotoned, the resulting anion quinolin-8-olate acts as a strong bidentate ligand. The quinolin-8-olate is able to bind metal cations very effectively, and its chelating power is considered second only to EDTA.[4] A quantitative insight into its electron density distribution can be of help in clarifying the nature of the metal−ligand interactions in these complexes. The analysis of the topological of electron charge density has proved to be a very powerful tool for studying a variety of metal−ligand and many other bonds.[5−7] The determination of $\rho(\mathbf{r})$ and its gradient field allows a network of atomic interaction lines to be established and permits each atomic interaction type to be accurately quantified. To obtain such information about the charge distribution of complexes of 8HQ with transition metals, a study on the topology of molecular charge distribution of complexes with Mn(III), Fe(III), and Co(III) ions, using the quantum theory of atoms in molecules,[8,9] was performed.

Topology of the Charge Distribution

The topology of $\rho(\mathbf{r})$ are summarized in its critical points,[8,9] ($\tilde{\mathbf{N}}\rho(\mathbf{r}_c) = 0$). The interaction of two atoms in a molecule leads to the formation of a bond critical point BCP in $\rho(\mathbf{r})$. [8,9] The $\tilde{\mathbf{N}}\rho(\mathbf{r})$ trajectories that originate and conclude at this point define, respectively, the bond path BP and the interatomic surface (IAS).[8,9] A chemical bond between two atoms is characterized by a line of maximum electron density, the BP, which links the two nuclei and intersects the IAS at a saddle critical point. The nature of the interaction between atoms is reflected on which of the curvatures of ρ dominates.[10] *Shared* interactions (covalent bonds) are dominated by the negative curvatures. In this case, ρ is concentrated in the internuclear region as a result of the perpendicular contractions toward the BP. This is reflected in a large value of $\rho(\mathbf{r}_c)$ and in a negative one for $\nabla^2\rho(\mathbf{r}_c)$. For *closed-shell* interactions (i.e., ionic and H bonds), the positive curvature of ρ along the BP is dominant. In this case, ρ is depleted in the IAS as a result of its contraction toward the nuclei.[10] They are characterized by a low value of $\rho(\mathbf{r}_c)$ and by a positive one for $\nabla^2\rho(\mathbf{r}_c)$. Most bonds studied are found between these two limits. [10]

Computational Methods

Single-point calculations were performed with Gaussian 03[11] employing a hybrid B3YLP functional[12] and a 6-311+G(d,p) basis set. The electron density $\rho(\mathbf{r})$, the gradient vector field $\nabla\rho(\mathbf{r})$, the associated Laplacian $\nabla^2\rho(\mathbf{r})$ scalar field, the critical points in $\rho(\mathbf{r})$, the interatomic surfaces and the bond paths were determined with local variations of the programs Morphy 98[13] and ProMolden 1.1.[14] The program[15] AIM2000 was employed to check the results obtained with the other programs and for the generation of molecular graphs and critical points.

The atomic coordinates in the metal complexes were obtained from the corresponding crystal structures. Previous crystal structures were used for Mn(III),[16] Fe(III),[17] and Co(III).[18]

Results and Discussion

In the complexes studied, each metal atom is coordinated by three 8HQ molecules.[16−18] All complexes showed remarkably similar structures thus facilitating their analysis. The N and O atoms of the 8HQ molecules are in close contact with the metal atom, forming dative bonds in a slightly distorted octahedral arrangement.[16−18] In Figure 1a, values of $\rho(\mathbf{r})$ in one molecular plane are shown together with the different IASs and all the BCPs present in free 8HQ. A comparison of Figures 1a and 2a showed the effects of metal coordination on the $\rho(\mathbf{r})$ of 8HQ. As expected, coordination changed the IAS of the atoms bonded to the metal. The shape and size of the basins of the O and N atoms were strongly modified and new ring critical points were

* To whom correspondence should be addressed. E-mail: jmurgich@ivic.ve.

† Universidad Central de Venezuela.

10.1021/jp9003054 CCC: $40.75
Published on Web 04/07/2009

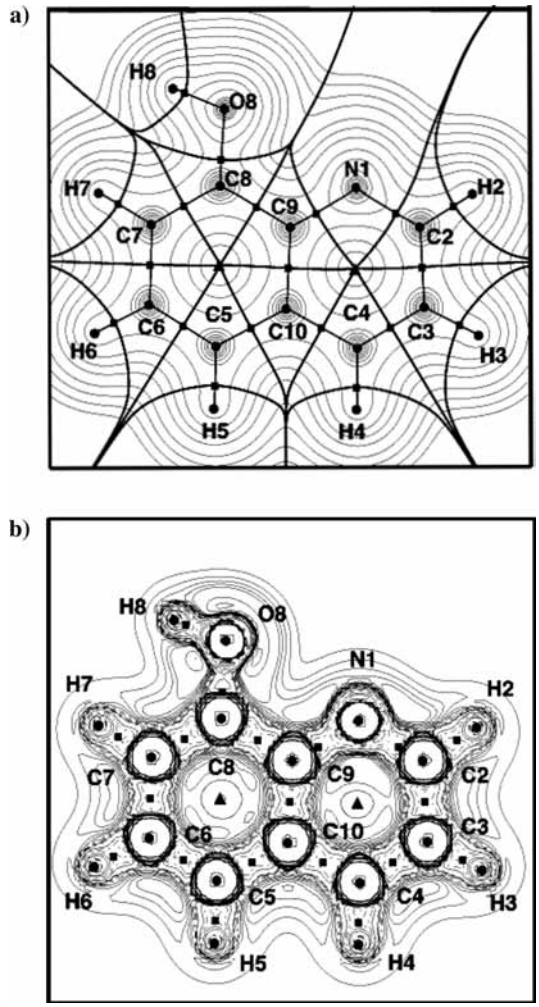

Figure 1. a) The bond paths, bond critical points [■], ring critical points [▲], and interatomic surfaces (in bold) superimposed on the electron density isocontour lines in the molecular plane of free 8HQ. (b) Distribution of the Laplacian of $\rho(\mathbf{r})$ in the same molecular plane.

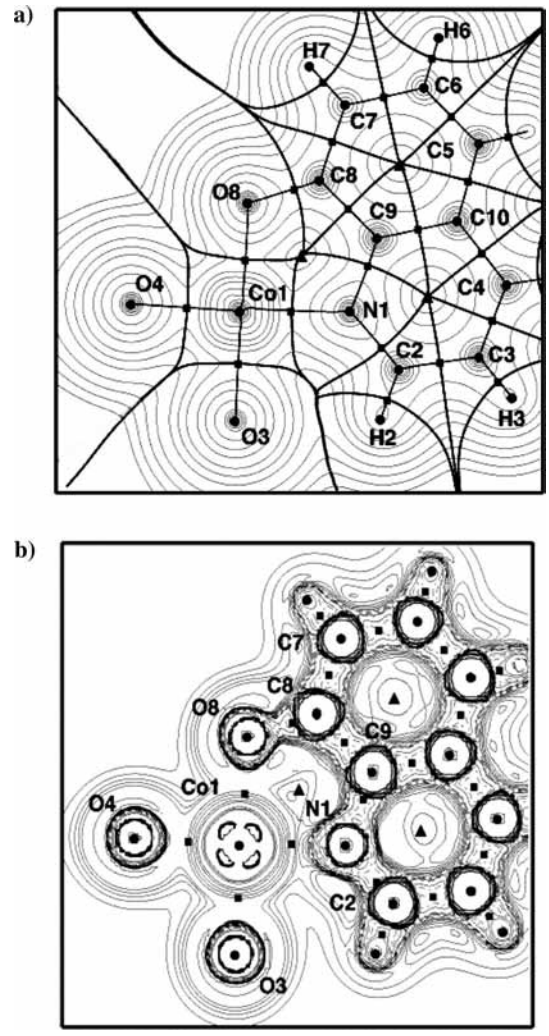

Figure 2. (a) The bond paths, bond critical points [■], ring critical points [▲], and interatomic surfaces (in bold) superimposed on the electron density isocontour lines in one molecular plane of the Co(III) complex of 8HQ. (b) Distribution of the Laplacian of $\rho(\mathbf{r})$ in the same molecular plane.

generated inside the polygons formed by the N, Metal, O8, C8, and C9 atoms (Figures 1a and 2a). The metal atoms were inside slightly distorted cubes generated by the IASs as seen in Figure 2a for the Co(III) complex.

The position of the BCPs and the values of $\rho(\mathbf{r}_c)$ and $\nabla^2\rho(\mathbf{r}_c)$ of the different bonds in free 8HQ are typical of substituted aromatic hydrocarbons. They correspond to covalent bonds between C, H, N, and O atoms in these molecules[19] (See Table 1). Further information about $\rho(\mathbf{r})$ may be obtained from the $\nabla^2\rho(\mathbf{r})$ distribution (Figure 1b). In the valence shell charge concentration (VSCC) of the N atom, a local concentration in the molecular plane corresponding to a classical "lone pair" was found for free 8HQ. Two similar concentrations were obtained in the O atom, but located symmetrically below and above the molecular plane of Figure 1a.

Figure 2b shows the effects of the coordination with Co(III) on the $\rho(\mathbf{r})$ distribution in a plane containing a 8HQ molecule, two O atoms from the other remaining molecules and the metal atom. The values of $\nabla^2\rho(\mathbf{r})$ in this plane showed that noticeable changes were present, mainly in the N and O atoms. Figure 3a shows the BPs found for the Co(III) complex. A similar set was obtained for the Mn(III) complex and is not shown for sake of brevity. For the Fe(III) complex, three additional bond paths linking the N atom of one of the 8HQ with one of the H atoms of a neighboring molecule (see Figure 3b) were found. These bonds were extremely weak intermolecular H bonds[20] ($\rho(\mathbf{r}_c)$ = 0.007, 0.008, and 0.009 au; $\nabla^2\rho(\mathbf{r}_c)$ = 0.028, 0.032, and 0.034 au). They also generated a few extra BCPs and some ring CPs as shown in Figure 3b. These weak H bonds did not perturb the neighboring ones so they were not analyzed further.

The values of $\nabla^2\rho(\mathbf{r})$ showed that the charge distribution for the Co(III) atom was such that eight nonbonded charge concentration in its VSCC were located at the corners of a cube and a depletion region was located in each of its six faces.[5] In Figure 2b is shown a plane containing the center of this cube. There, one may distinguish four semicircles corresponding to the charge concentrations found at the four edges and, also, four depletion regions in the faces of the cube of the VSCC of Co. Similar graphs for the charge distribution of the Mn(III) and Fe(III) atoms were found in this plane. This particular type of metal charge distribution was similar to those found for coordinated Co(III) in several squarates[21] and in complexes of aromatic amino acids,[22] for Fe(III) in $Fe_2(CO)_9$[6] and for Cr(III) in $Cr(CO)_6$.[7]

The effects of the metal coordination was also reflected in $\rho(\mathbf{r}_c)$ and $\nabla^2\rho(\mathbf{r}_c)$ of the other bonds of the 8HQ molecules. Equivalent bonds of these molecules showed slightly different

TABLE 1: Properties of Bond Critical Points of 8HQ[a]

property	bonds						
bond	O8—H8	O8—C8	C8—C9	C9—N1	N1—C2	C2—C3	
$\rho(\mathbf{r}_c)$	0.360	0.289	0.295	0.326	0.352	0.298	
$\nabla^2\rho(\mathbf{r}_c)$	−2.448	−0.382	−0.805	−0.969	−0.946	−0.813	
bond	C3—C4	C10—C4	C10—C9	C10—C5	C5—C6	C6—C7	C7—C8
$\rho(\mathbf{r}_c)$	0.320	0.296	0.292	0.295	0.319	0.296	0.317
$\nabla^2\rho(\mathbf{r}_c)$	−0.916	−0.806	−0.769	−0.794	−0.903	−0.796	−0.892
bond	C7—H7	C6—H6	C5—H5	C4—H4	C3—H3	C2—H2	
$\rho(\mathbf{r}_c)$	0.276	0.281	0.279	0.280	0.280	0.283	
$\nabla^2\rho(\mathbf{r}_c)$	−0.928	−0.962	−0.946	−0.962	−0.960	−0.982	

[a] The values of $\rho(\mathbf{r})$ and $\nabla^2\rho(\mathbf{r}_c)$ are in au.

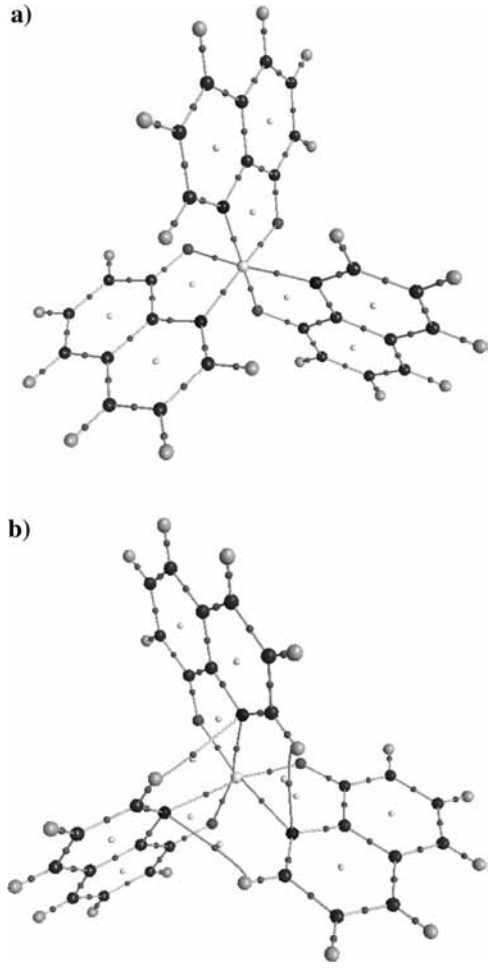

Figure 3. (a) 3-D molecular graph of the Co(III) complex of 8HQ. The small dark spheres in the bonds show the position of the bond critical points while the lighter ones correspond to the ring critical points. (b) 3-D molecular graph of the Fe(III) complex of 8HQ showing the extra H bonds and the bond and ring critical points as in part a.

values for both $\rho(\mathbf{r}_c)$ and $\nabla^2\rho(\mathbf{r}_c)$ (Tables 2−4). These changes were quite small and mainly reflected minor perturbations on $\rho(\mathbf{r}_c)$ and $\nabla^2\rho(\mathbf{r}_c)$ within the set studied. Similar changes in equivalent bonds were found in their $\rho(\mathbf{r}_c)$ and $\nabla^2\rho(\mathbf{r}_c)$ values obtained[23] for 1,8-bis(dimethyl-amino)naphthalene DMAN. These small changes were attributed to the effects of the variations in the crystal field within the complex on the $\rho(\mathbf{r})$ of equivalent bonds within the unit cell. Therefore, it is reasonable to assume that the small asymmetries found in the charge distribution of equivalent bonds of the 8HQ molecules are likely to be produced by the variation in the crystal field within the volume of the complex. As we were mainly interested in the large changes generated by metal coordination, only the average values of both $\rho(\mathbf{r}_c)$ and $\nabla^2\rho(\mathbf{r}_c)$ for each of the different bonds of 8HQ were used in our analysis (Table 5).

In the metal complexes of 8HQ, the regions of VSCC of the N atoms were directed toward depletion regions of the metal ion as shown in Figure 2b for the Co(III) complex. The electron-rich regions of the ligands were found to face regions of low concentration occurring on the six faces of the cube describing the charge concentration of the Co(III) atom. Therefore, the coordination of the 8HQ molecule can be represented as a set of regions of charge concentration of the ligands matching the depletion regions of the VSCC of the Co(III) atoms. The same conclusion was drawn for the Mn(III) and Fe(III) complexes of 8HQ where similar charge distributions were found for metal−ligand coordination. The characteristics of the critical points of the metal−N and metal−O bonds are shown in Table 5. The changes in the O charge distribution were quite significant as a result of the transformation a covalent O−H bond of 8HQ onto a dative one with the metal. In the covalent case, a large value for $\rho(\mathbf{r}_c)$ and a high and negative one for $\nabla^2\rho(\mathbf{r}_c)$ was found. These values are characteristics of a typical covalent O−H bond.[10] When the dative O−metal bond is formed, its $\rho(\mathbf{r}_c)$ decreases drastically to less than $\sim^1/_3$ of its covalent value while the $\nabla^2\rho(\mathbf{r}_c)$ changes its sign and decreases significantly in absolute value. The values of $\rho(\mathbf{r}_c)$ for O−metal bonds were quite similar for the Mn(III) and Co(III) complexes with a slightly smaller one for the O−Fe(III) bond. Similarly, for the N−metal bonds the values were quite close for the Mn(III) and Co(III) complexes, while for Fe(III), a ∼29% lower value was obtained (Table 5).

Valuable additional information on chemical bond properties is available from the total electron energy density,[6] $H(\mathbf{r}_c)$. This is particularly important for dative bonds where the value of $\nabla^2\rho(\mathbf{r}_c)$ not always provides a unambiguous picture of the type of bond present. The energy density is such that $H(\mathbf{r}_c) = G(\mathbf{r}_c) + V(\mathbf{r}_c)$, where $G(\mathbf{r}_c)$, is the kinetic electron energy density and $V(\mathbf{r}_c)$ is the potential electron energy density.[6]The charge density parameters at the BCPs are related with local energy densities by means of the following equations: $G(\mathbf{r}_c) = (^3/_{10})(3\pi^2)^{2/3}\rho^{5/3}(\mathbf{r}_c) + (^1/_6)\nabla^2\rho(\mathbf{r}_c)$ and $(^1/_4)\nabla^2\rho(\mathbf{r}_c) = 2G(\mathbf{r}_c) + V(\mathbf{r}_c)$. Abramov[24] proposed the first equation for the kinetic energy density along BPs of both open and closed-shell interactions. The second one was obtained from the expression of the local virial theorem.[9] The values and sign of $H(\mathbf{r}_c)$ has been used to accurately classify different bonded interactions.[9,10] When $V(\mathbf{r}_c) < 0$ and $|V(\mathbf{r}_c)| > G(\mathbf{r}_c)$ such that $H(\mathbf{r}_c)$ is negative, a bonded interaction is defined as a shared (covalent) interaction. When $|V(\mathbf{r}_c)| < G(\mathbf{r}_c)$, it is defined as a closed-shell interaction.[6,9] In Table 6 are shown the values obtained for the dative bonds found in the complexes of 8HQ. The values of $H(\mathbf{r}_c)$ found for them were all small and negative. This means that $|V(\mathbf{r}_c)|$ is only slightly larger than $G(\mathbf{r}_c)$ so these dative bonds are intermediate between closed-shell and shared interaction. This was further confirmed by the fact that the values[6] of $G(\mathbf{r}_c)/\rho(\mathbf{r}_c)$ were

TABLE 2: Properties of Bond Critical Points of Mn(III) 8HQ[a]

property	bonds molecule 1						
bond	O8—Mn1	N1—Mn1	O8—C8	C8—C9	C9—N1	N1—C2	C2—C3
$\rho(\mathbf{r}_c)$	0.099	0.107	0.313	0.307	0.315	0.331	0.307
$\nabla^2\rho(\mathbf{r}_c)$	0.515	0.471	−0.574	−0.879	−0.816	−0.768	−0.866
bond	C3—C4	C4—C10	C10—C9	C10—C5	C5—C6	C6—C7	C7—C8
$\rho(\mathbf{r}_c)$	0.337	0.305	0.315	0.295	0.326	0.302	0.320
$\nabla^2\rho(\mathbf{r}_c)$	−1.024	−0.860	−0.910	−0.798	−0.951	−0.831	−0.928
bond	C7—H7	C6—H6	C5—H5	C4—H4	C3—H3	C2—H2	
$\rho(\mathbf{r}_c)$	0.388	0.391	0.386	0.392	0.390	0.400	
$\nabla^2\rho(\mathbf{r}_c)$	−1.758	−1.787	−1.731	−1.805	−1.779	−1.900	
property	bonds molecule 2						
bond	O8—Mn1	N1—Mn1	O8—C8	C8—C9	C9—N1	N1—C2	C2—C3
$\rho(\mathbf{r}_c)$	0.099	0.102	0.322	0.305	0.310	0.336	0.304
$\nabla^2\rho(\mathbf{r}_c)$	0.530	0.480	−0.508	−0.863	−0.820	−0.766	−0.847
bond	C3—C4	C4—C10	C10—C9	C10—C5	C5—C6	C6—C7	C7—C8
$\rho(\mathbf{r}_c)$	0.329	0.303	0.300	0.304	0.319	0.303	0.315
$\nabla^2\rho(\mathbf{r}_c)$	−0.975	−0.852	−0.826	−0.845	−0.912	−0.829	−0.903
bond	C7—H7	C6—H6	C5—H5	C4—H4	C3—H3	C2—H2	
$\rho(\mathbf{r}_c)$	0.389	0.391	0.387	0.392	0.390	0.400	
$\nabla^2\rho(\mathbf{r}_c)$	−1.764	−1.790	−1.736	−1.803	−1.777	−1.893	
property	bonds molecule 3						
bond	O8—Mn1	N1—Mn1	O8—C8	C8—C9	C9—N1	N1—C2	C2—C3
$\rho(\mathbf{r}_c)$	0.105	0.102	0.313	0.305	0.311	0.337	0.311
$\nabla^2\rho(\mathbf{r}_c)$	0.536	0.465	−0.574	−0.869	−0.809	−0.772	−0.886
bond	C3—C4	C4—C10	C10—C9	C10—C5	C5—C6	C6—C7	C7—C8
$\rho(\mathbf{r}_c)$	0.325	0.297	0.304	0.298	0.324	0.302	0.315
$\nabla^2\rho(\mathbf{r}_c)$	−0.950	−0.813	−0.850	−0.814	−0.944	−0.827	−0.900
bond	C7—H7	C6—H6	C5—H5	C4—H4	C3—H3	C2—H2	
$\rho(\mathbf{r}_c)$	0.388	0.391	0.386	0.392	0.389	0.397	
$\nabla^2\rho(\mathbf{r}_c)$	−1.757	−1.793	−1.722	−1.805	−1.771	−1.860	

[a] The values of $\rho(\mathbf{r})$ and $\nabla^2\rho(\mathbf{r}_c)$ are in au.

TABLE 3: Properties of Bond Critical Points of Fe(III) 8HQ[a]

property	bonds molecule 1						
bond	O8—Fe1	N1—Fe1	O8—C8	C8—C9	C9—N1	N1—C2	C2—C3
$\rho(\mathbf{r}_c)$	0.099	0.058	0.316	0.305	0.313	0.353	0.281
$\nabla^2\rho(\mathbf{r}_c)$	0.483	0.260	−0.516	−0.864	−0.834	−0.780	−0.715
bond	C3—C4	C4—C10	C10—C9	C10—C5	C5—C6	C6—C7	C7—C8
$\rho(\mathbf{r}_c)$	0.332	0.295	0.309	0.312	0.330	0.300	0.323
$\nabla^2\rho(\mathbf{r}_c)$	−0.989	−0.803	−0.877	−0.894	−0.983	−0.758	−0.952
bond	C7—H7	C6—H6	C5—H5	C4—H4	C3—H3	C2—H2	
$\rho(\mathbf{r}_c)$	0.289	0.376	0.371	0.376	0.374	0.381	
$\nabla^2\rho(\mathbf{r}_c)$	−1.017	−1.676	−1.616	−1.683	−1.657	−1.732	
property	bonds molecule 2						
bond	O8—Fe1	N1—Fe1	O8—C8	C8—C9	C9—N1	N1—C2	C2—C3
$\rho(\mathbf{r}_c)$	0.092	0.058	0.330	0.299	0.308	0.362	0.298
$\nabla^2\rho(\mathbf{r}_c)$	0.423	0.240	−0.438	−0.831	−0.829	−0.741	−0.813
bond	C3—C4	C4—C10	C10—C9	C10—C5	C5—C6	C6—C7	C7—C8
$\rho(\mathbf{r}_c)$	0.333	0.298	0.316	0.301	0.342	0.283	0.315
$\nabla^2\rho(\mathbf{r}_c)$	−0.997	−0.821	−0.915	−0.834	−1.056	−0.716	−0.898
bond	C7—H7	C6—H6	C5—H5	C4—H4	C3—H3	C2—H2	
$\rho(\mathbf{r}_c)$	0.288	0.375	0.370	0.376	0.373	0.381	
$\nabla^2\rho(\mathbf{r}_c)$	−1.015	−1.668	−1.608	−1.686	−1.647	−1.725	
property	bonds molecule 3						
bond	O8—Fe1	N1—Fe1	O8—C8	C8—C9	C9—N1	N1—C2	C2—C3
$\rho(\mathbf{r}_c)$	0.090	0.061	0.315	0.307	0.314	0.347	0.305
$\nabla^2\rho(\mathbf{r}_c)$	0.424	0.249	−0.565	−0.877	−0.833	−0.801	−0.851
bond	C3—C4	C4—C10	C10—C9	C10—C5	C5—C6	C6—C7	C7—C8
$\rho(\mathbf{r}_c)$	0.316	0.319	0.291	0.328	0.329	0.293	0.333
$\nabla^2\rho(\mathbf{r}_c)$	−0.898	−0.944	−0.776	−1.002	−0.975	−0.776	−1.013
bond	C7—H7	C6—H6	C5—H5	C4—H4	C3—H3	C2—H2	
$\rho(\mathbf{r}_c)$	0.289	0.374	0.371	0.376	0.374	0.380	
$\nabla^2\rho(\mathbf{r}_c)$	−1.019	−1.665	−1.620	−1.687	−1.659	−1.722	

[a] The values of $\rho(\mathbf{r})$ and $\nabla^2\rho(\mathbf{r}_c)$ are in au.

TABLE 4: Properties of Bond Critical Points of Co(III) 8HQ[a]

property	bonds molecule 1						
bond	O8−Co1	N1−Co1	O8−C8	C8−C9	C9−N1	N1−C2	C2−C3
$\rho(\mathbf{r}_c)$	0.105	0.102	0.327	0.305	0.311	0.337	0.311
$\nabla^2\rho(\mathbf{r}_c)$	0.536	0.465	−0.485	−0.869	−0.809	−0.772	−0.886
bond	C3−C4	C4−C10	C10−C9	C10−C5	C5−C6	C6−C7	C7−C8
$\rho(\mathbf{r}_c)$	0.325	0.297	0.304	0.298	0.324	0.302	0.315
$\nabla^2\rho(\mathbf{r}_c)$	−0.920	−0.813	−0.850	−0.814	−0.944	−0.827	−0.901
bond	C7−H7	C6−H6	C5−H5	C4−H4	C3−H3	C2−H2	
$\rho(\mathbf{r}_c)$	0.388	0.391	0.386	0.392	0.389	0.397	
$\nabla^2\rho(\mathbf{r}_c)$	−1.757	−1.793	−1.722	−1.805	−1.771	−1.860	
property	bonds molecule 2						
bond	O8−Co1	N1−Co1	O8−C8	C8−C9	C9−N1	N1−C2	C2−C3
$\rho(\mathbf{r}_c)$	0.099	0.107	0.313	0.307	0.315	0.331	0.307
$\nabla^2\rho(\mathbf{r}_c)$	0.515	0.472	−0.574	−0.879	−0.816	−0.768	−0.866
bond	C3−C4	C4−C10	C10−C9	C10−C5	C5−C6	C6−C7	C7−C8
$\rho(\mathbf{r}_c)$	0.337	0.305	0.298	0.295	0.326	0.302	0.320
$\nabla^2\rho(\mathbf{r}_c)$	−1.024	−0.860	−0.814	−0.796	−0.951	−0.831	−0.928
bond	C7−H7	C6−H6	C5−H5	C4−H4	C3−H3	C2−H2	
$\rho(\mathbf{r}_c)$	0.388	0.391	0.386	0.392	0.390	0.400	
$\nabla^2\rho(\mathbf{r}_c)$	−1.758	−1.787	−1.731	−1.805	−1.779	−1.900	
property	bonds molecule 3						
bond	O8−Co1	N1−Co1	O8−C8	C8−C9	C9−N1	N1−C2	C2−C3
$\rho(\mathbf{r}_c)$	0.099	0.102	0.322	0.305	0.310	0.336	0.304
$\nabla^2\rho(\mathbf{r}_c)$	0.530	0.480	−0.553	−0.863	−0.820	−0.766	−0.847
bond	C3−C4	C4−C10	C10−C9	C10−C5	C5−C6	C6−C7	C7−C8
$\rho(\mathbf{r}_c)$	0.329	0.303	0.300	0.304	0.319	0.303	0.315
$\nabla^2\rho(\mathbf{r}_c)$	−0.975	−0.852	−0.826	−0.845	−0.912	−0.829	−0.903
bond	C7−H7	C6−H6	C5−H5	C4−H4	C3−H3	C2−H2	
$\rho(\mathbf{r}_c)$	0.389	0.391	0.387	0.392	0.389	0.400	
$\nabla^2\rho(\mathbf{r}_c)$	−1.764	−1.790	−1.736	−1.803	−1.777	−1.893	

[a] The values of $\rho(\mathbf{r})$ and $\nabla^2\rho(\mathbf{r}_c)$ are in au.

all >1, the $\rho(\mathbf{r}_c)$ values were all rather small when compared with those found for covalent bonds but still quite significant when compared with pure closed shell (ionic) bonds. The values of $\nabla^2\rho(\mathbf{r}_c)$ for the dative bonds were all positive as in closed-shell interactions.[5,6,9] These results obtained for the dative bonds of 8HQ are in excellent agreement with measurements and/or calculations made for the[25] Ti−C and[26] Mn−C dative bonds in several Ti and Mn complexes.[27]

The changes in $\rho(\mathbf{r}_c)$ and $\nabla^2\rho(\mathbf{r}_c)$ for the other bonds of the 8HQ molecules not directly involved in the coordination were quite subtle. From Figures 1 and 2, we expected that the C−N and the O−C bonds should be the most perturbed. Other more distant bonds are also perturbed by the coordination but to a much smaller degree than the C−N and O−C ones. The O8−C8 and C9−C8 bonds showed a larger density at the BCP and a slightly more negative value for the $\nabla^2\rho(\mathbf{r}_c)$ upon coordination. This showed a net reinforcement of these covalent bonds upon complex formation. This is a direct result of the changes produced in the O VSCC charge distribution when the metal replaced the H atom. On the other hand, $\rho(\mathbf{r}_c)$ decreased for both N−C bonds except for the N−C2 one in the Fe complex. The coordination of the N "lone pair" with the metal atom seemed to increase the ability of its VSCC to withdraw charge from the N−C bond regions thus depleting $\rho(\mathbf{r}_c)$. The $\nabla^2\rho(\mathbf{r}_c)$ also decreased in absolute value in these bonds showing a trend toward a more intermediate character. For the C−C bonds, the changes produced by the metal coordination were quite small and did not seem to follow any simple trend (see Table 5). The most important changes found upon complex formation in the rest of the 8HQ molecule were located in the C−H bonds. The only exception was the C7−H7 bond in the Fe complex where a smaller variation was found in $\rho(\mathbf{r}_c)$ than in the other ones. In all the other C−H bonds, a noticeable increase in $\rho(\mathbf{r}_c)$ (∼30%) and $\nabla^2\rho(\mathbf{r}_c)$ (∼80%) was observed upon metal coordination. These changes showed a noticeable increase in the C−H bond strength upon metal coordination.

The Mn(III) and Co(III) complexes consistently showed very similar trends for the different bonds of 8HQ molecule while the Fe(III) complex gave always slightly smaller changes. Nevertheless, the trend found in the Fe(III) complex followed that of the other two metals.

Recently, the values of $\rho(\mathbf{r}_c)$ at the C−C bonds in aromatic hydrocarbons were correlated with the electron delocalization δ(A,B) index in aromatic hydrocarbons.[19] It was shown that when δ(A,B) is used to count the number of electron pairs shared between bonded atoms A and B it can be interpreted as a bond order when no significant charge transfer exists between them.[19] It seemed reasonable to extend the use of the correlation found between $\rho(\mathbf{r}_c)$ and $\delta(C_A,C_B)$ in polyaromatic hydrocarbons although limiting its use to only the C−C bonds present in 8HQ. In Table 6 are shown the results obtained for the C−C bonds in free and coordinated 8HQ. As expected, the values of $\delta(C_A,C_B)$ are not symmetric due to the presence of the N atom within one of the ring system and also from the effects of the OH substitution at C8 in 8HQ. In general, the changes found in bond orders were similar for the three metal complexes. As expected, the 8HQ molecule in the Fe(III) complex showed a slightly different behavior than in the other two complexes. The metal coordination increased the order of C9−C8 bond by 6% while the C10−C9 increased in the order Mn(III) > Fe(III) > Co(III) by a smaller amount. The C−C bonds of 8HQ in the Mn(III) and Co(III) complexes showed practically identical changes except for the bridging C10−C9 bond where a noticeable difference was found. A comparison of the values

TABLE 5: Average Properties of Bond Critical Points of free 8HQ and Mn, Fe, and Co 8-HQs[a]

property	bonds free 8HQ						
bond	O8—H8	O8—C8	C9—C8	C9—N1	C2—N1	C3—C2	
$\rho(\mathbf{r}_c)$	0.360	0.289	0.295	0.326	0.352	0.298	
$\nabla^2\rho(\mathbf{r}_c)$	−2.448	−0.382	−0.805	−0.969	−0.946	−0.813	
bond	C4—C3	C10—C4	C10—C9	C10—C5	C6—C5	C7—C6	C8—C7
$\rho(\mathbf{r}_c)$	0.320	0.296	0.292	0.295	0.319	0.296	0.317
$\nabla^2\rho(\mathbf{r}_c)$	−0.916	−0.806	−0.769	−0.794	−0.903	−0.796	−0.892
bond	C7—H7	C6—H6	C5—H5	C4—H4	C3—H3	C2—H2	
$\rho(\mathbf{r}_c)$	0.276	0.281	0.279	0.280	0.280	0.283	
$\nabla^2\rho(\mathbf{r}_c)$	−0.928	−0.962	−0.946	−0.962	−0.960	−0.982	
property	bonds mean values Mn						
bond	O8—Mn1	N1—Mn1	O8—C8	C8—C9	C9—N1	N1—C2	C2—C3
$\rho(\mathbf{r}_c)$	0.101	0.104	0.316	0.306	0.312	0.335	0.307
$\nabla^2\rho(\mathbf{r}_c)$	0.527	0.472	−0.576	−0.870	−0.815	−0.769	−0.866
bond	C3—C4	C4—C10	C10—C9	C10—C5	C5—C6	C6—C7	C7—C8
$\rho(\mathbf{r}_c)$	0.330	0.302	0.306	0.299	0.323	0.302	0.317
$\nabla^2\rho(\mathbf{r}_c)$	−0.983	−0.842	−0.862	−0.819	−0.937	−0.829	−0.910
bond	C7—H7	C6—H6	C5—H5	C4—H4	C3—H3	C2—H2	
$\rho(\mathbf{r}_c)$	0.388	0.391	0.386	0.392	0.390	0.399	
$\nabla^2\rho(\mathbf{r}_c)$	−1.760	−1.790	−1.730	−1.804	−1.776	−1.884	
property	bonds mean values Fe						
bond	O8—Fe1	N1—Fe1	O8—C8	C8—C9	C9—N1	N1—C2	C2—C3
$\rho(\mathbf{r}_c)$	0.094	0.059	0.320	0.304	0.312	0.354	0.295
$\nabla^2\rho(\mathbf{r}_c)$	0.443	0.250	−0.506	−0.857	−0.832	−0.774	−0.793
bond	C3—C4	C4—C10	C10—C9	C10—C5	C5—C6	C6—C7	C7—C8
$\rho(\mathbf{r}_c)$	0.327	0.304	0.305	0.314	0.334	0.292	0.324
$\nabla^2\rho(\mathbf{r}_c)$	−0.961	−0.856	−0.856	−0.910	−1.005	−0.750	−0.954
bond	C7—H7	C6—H6	C5—H5	C4—H4	C3—H3	C2—H2	
$\rho(\mathbf{r}_c)$	0.289	0.375	0.371	0.376	0.374	0.381	
$\nabla^2\rho(\mathbf{r}_c)$	−1.017	−1.700	−1.615	−1.685	−1.654	−1.726	
property	bonds mean values Co						
bond	O8—Co1	N1—Co1	O8—C8	C8—C9	C9—N1	N1—C2	C2—C3
$\rho(\mathbf{r}_c)$	0.101	0.104	0.321	0.306	0.312	0.335	0.307
$\nabla^2\rho(\mathbf{r}_c)$	0.527	0.472	−0.537	−0.870	−0.815	−0.769	−0.866
bond	C3—C4	C4—C10	C10—C9	C10—C5	C5—C6	C6—C7	C7—C8
$\rho(\mathbf{r}_c)$	0.330	0.302	0.301	0.299	0.323	0.302	0.317
$\nabla^2\rho(\mathbf{r}_c)$	−0.973	−0.842	−0.830	−0.818	−0.936	−0.829	−0.911
bond	C7—H7	C6—H6	C5—H5	C4—H4	C3—H3	C2—H2	
$\rho(\mathbf{r}_c)$	0.388	0.391	0.386	0.392	0.389	0.399	
$\nabla^2\rho(\mathbf{r}_c)$	−1.760	−1.790	−1.730	−1.804	−1.776	−1.884	

[a] The values of $\rho(\mathbf{r})$ and $\nabla^2\rho(\mathbf{r}_c)$ are in au.

TABLE 6: Calculated Local Energy Density Properties for Mn−O, Mn−N, Fe−O, Fe−N, Co−N, and Co−O Bonded Interactions[a]

bond	$G(\mathbf{r}_c)$	$G(\mathbf{r}_c)/\rho(\mathbf{r}_c)$	$V(\mathbf{r}_c)$	$H(\mathbf{r}_c)$
O−Mn	0.151	1.50	−0.170	−0.019
N−Mn	0.145	1.39	−0.172	−0.027
O−Fe	0.130	1.38	−0.140	−0.010
N−Fe	0.067	1.14	−0.072	−0.005
O−Co	0.151	1.50	−0.170	−0.019
N−Co	0.145	1.39	−0.172	−0.027

[a] The values of $\rho(\mathbf{r})$ and $\nabla^2\rho(\mathbf{r}_c)$ are in au.

of $\delta(C_A,C_B)$ for benzene[19] with those of free 8HQ and its complexes showed that aromaticity slightly increased in the C−C bonds as the metal interacts with the N and O atoms except for the C3−C2 and C7−C6 bond in the Fe(III) complex where a rather small decrease was found, instead.

Conclusions

It was found that the metal charge distribution in the complexes of 8HQ showed eight nonbonded charge concentrations in its VSCC that were located at the corners of a cube and a depletion region that was located in each of its six faces. The coordination of the 8HQ was such that a set of regions of charge concentration of the ligands matched the depletion regions of the cube of charge of the metal atoms. The O− and N−metal dative bonds exhibited low values for $\rho(\mathbf{r}_c)$ and

TABLE 7: Values of the Delocalization Index $\delta(C_A,C_B)$ for the Different C−C Bonds of 8HQ[a]

	C2−C3	C3−C4	C10−C4	C10−C9	C10−C5	C5−C6	C6−C7	C7−C8	C9−C8
8HQ	1.170	1.331	1.157	1.130	1.150	1.324	1.157	1.308	1.150
Mn8HQ	1.234	1.412	1.198	1.227	1.177	1.355	1.197	1.308	1.227
Fe8HQ	1.150	1.387	1.212	1.219	1.285	1.445	1.130	1.363	1.212
Co8HQ	1.234	1.412	1.198	1.191	1.177	1.355	1.198	1.308	1.227

[a] The values of $\rho(\mathbf{r})$ and $\nabla^2\rho(\mathbf{r}_c)$ are in au.

positive ones for $\nabla^2\rho(\mathbf{r}_c)$ showing that the atoms were linked by a closed shell interaction containing some covalent character.

The most important changes were located around the N and O atoms of 8HQ directly involved in dative bonds with the metal ion. Significant changes were also found in $\rho(\mathbf{r}_c)$ of bonds connecting these atoms with neighboring C−C bonds with respect to free 8HQ. By use of the $\delta(C_A,C_B)$ values, it was shown that complexation increased the aromaticity of most C−C bonds with only two exceptions. The most important changes in $\rho(\mathbf{r}_c)$ and $\nabla^2\rho(\mathbf{r}_c)$ were found in the C−H bonds were an increase in bond strength was obtained upon complexation.

Acknowledgment. To Professors P.L.A. Popelier from University of Manchester, United Kingdom, and A. Martín Pendás from University of Oviedo, Spain, for kindly providing the Morphy 98 and ProMolden 1.1 programs, respectively.

References and Notes

(1) Soroka, K.; Vithanage, R. S.; Phillips, D. A.; Walker, B.; Dasgupta, P. K. *Anal. Chem.* **1987**, *59*, 629.

(2) Hollingshead, R. G. W. *Oxine and Its Derivatives*; Butterworths: London, **1954**−**1956**; Vols. *I*−*IV*.

(3) Phillips, J. P. *Chem. Rev.* **1955**, *56*, 271. Hollingshead, R. G. W. *Anal. Chim. Acta* **1958**, *19*, 447. Dowlings, S. D.; Seitz, W. R. *Spectrochim. Acta* **1984**, *40A*, 991. Farruggia, G.; Iotti, S.; Prodi, L.; Montalti, M.; Zaccheroni, N.; Savage, P. B.; Trapani, V.; Sale, P.; Wolf, F. I. *J. Am. Chem. Soc.* **2006**, *128*, 344..

(4) Sheats, J. R.; Antoniadis, H.; Hueschen, M.; Leonard, W.; Miller, J.; Moon, R.; Roitman, D.; Stocking, A. *Science* **1996**, *273*, 884. Amati, M.; Lelj, F. *J. Phys. Chem. A* **2003**, *107*, 2560. Amati, M.; Belviso, S.; Cristinziano, P. L.; Minichino, C.; Lelj, F.; Aiello, I.; La Deda, M.; Ghedini, M. *J. Phys. Chem. A* **2007**, *111*, 13403−13414–13403.

(5) MacDougall, P. J.; Hall, M. B. *Trans. Am. Crystallogr. Assoc.* **1990**, *26*, 105–123.

(6) Macchi, P.; Sironi, A. *Coord. Chem. Rev.* **2003**, *238/239*, 383–412.

(7) Cortes-Guzman, R. F. W.; Bader, *Coord. Chem. Rev.* **2005**, *249*, 633–662.

(8) Popelier, P. L. A. *Atoms in Molecules: An Introduction*; Prentice Hall: Edinburgh, 2000.

(9) Bader, R. F. W. *Atoms in Molecules A Quantum Theory*; Oxford University Press: Oxford, 1990.

(10) Bader, R. F. W.; Essen, H. *J. Chem. Phys.* **1984**, *80*, 1943–1960.

(11) Frisch, M. J.; Trucks, G. W.; Schlegel, H. B.; Scuseria, G. E.; Robb, M. A.; Cheeseman, J. R.; Montgomery, J. A., Jr.; Vreven, T.; Kudin, K. N.; Burant, J. C.; Millam, J. M.; Iyengar, S. S.; Tomasi, J.; Barone, V.; Mennucci, B.; Cossi, M.; Scalmani, G.; Rega, N.; Petersson, G. A.; Nakatsuji, H.; Hada, M.; Ehara, M.; Toyota, K.; Fukuda, R.; Hasegawa, J.; Ishida, M.; Nakajima, T.; Honda, Y.; Kitao, O.; Nakai, H.; Klene, M.; Li, X.; Knox, J. E.; Hratchian, H. P.; Cross, J. B.; Bakken, V.; Adamo, C.; Jaramillo, J.; Gomperts, R.; Stratmann, R. E.; Yazyev, O.; Austin, A. J.; Cammi, R.; Pomelli, C.; Ochterski, J. W.; Ayala, P. Y.; Morokuma, K.; Voth, G. A.; Salvador, P.; Dannenberg, J. J.; Zakrzewski, V. G.; Dapprich, S.; Daniels, A. D.; Strain, M. C.; Farkas, O.; Malick, D. K.; Rabuck, A. D.; Raghavachari, K.; Foresman, J. B.; Ortiz, J. V.; Cui, Q.; Baboul, A. G.; Clifford, S.; Cioslowski, J.; Stefanov, B. B.; Liu, G.; Liashenko, A.; Piskorz, P.; Komaromi, I.; Martin, R. L.; Fox, D. J.; Keith, T.; Al-Laham, M. A.; Peng, C. Y.; Nanayakkara, A.; Challacombe, M.; Gill, P. M. W.; Johnson, B.; Chen, W.; Wong, M. W.; Gonzalez, C.; Pople, J. A. *Gaussian 03*, revision B.04; Gaussian, Inc.: Wallingford, CT, 2004.

(12) Stephens, P. J.; Devlin, F. J.; Chablowski, C. F.; Frisch, M. J. *J. Phys. Chem.* **1994**, *98*, 11623–11627.

(13) Popelier, P. L. A.; Bone, R. G. A.; Popelier, P. L. A. *Comp. Phys. Commun.* **1996**, *93*, 212–240.

(14) Martin Pendás, A. *Promolden*, version 1.10(c); University of Oviedo: Spain, 2002. Available at http://web.uniovi.es/qcg/d-DensEl/.

(15) (a) Biegler-Köenig, F. W.; Schönbohm, J. *J. Comput. Chem.* **2002**, *23*, 1489–1494.

(16) Xjong, R. G.; You, X. Z. *Acta Crystallogr.* **1995**, *C51*, 1978–1980.

(17) Pech, L.; Bankovsky, Y. A.; Kemme, A.; Lejejs, J. *Acta Crystallogr.* **1997**, *C53*, 1043–1045.

(18) Li, D. X.; Xu, D. J.; Gu, J. M.; Xu, Y. Z. *Acta Crystallogr.* **2003**, *E59*, m543–m545.

(19) Matta, C. F.; Hernández-Trujillo, J. *J. Phys. Chem. A* **2003**, *107*, 7496–7504.

(20) Mata, I.; Alkorta, I.; Espinosa, E.; Molins, E.; Elguero, J. *The Quantum Theory of Atoms in Molecules*; Matta, C. F., Boyd, R. J. Eds.; Wiley-VCH Verlag: Weinheim, 2007.

(21) Lee, C. R.; Wang, C. C.; Chen, K. C.; Lee, G. S.; Wang, Y. *J. Phys. Chem. A* **1999**, *103*, 156–165.

(22) Overgaard, J.; Waller, R M.; Piltz, P.; Platts, J. A.; Emseis, P.; Leverett, P.; Williams, P. A.; Hibbs, D. E. *J. Phys. Chem. A* **2007**, *111*, 10123–10133.

(23) Mallinson, P. R.; Wozniak, K.; Wilson, C. C.; McCormack, K. L.; Yufit, D. S. *J. Am. Chem. Soc.* **1999**, *121*, 4640–4646.

(24) Abramov, Yu. A. *Acta Crystallogr.* **1997**, *A53*, 264–272.

(25) Bader, R. F. W.; Matta, C. F. *Inorg. Chem.* **2001**, *40*, 5603–5611.

(26) Abramov, Yu. A.; Brammer, L.; Klooster, W. T.; Bullock, R. M. *Inorg. Chem.* **1998**, *37*, 6317–6328.

(27) Koritsanszky, T. S.; Coppens, P. *Chem. Rev.* **2001**, *101*, 1583–1627.

JP9003054